minerals

MDPI

Article

Selective Inhibition Mechanisms of Fe(III) in the Flotation of Lepidolite

Feifan Wang [1,2,3,†], Lei Liu [1,4,†], Jingjing Zhang [2,3], Yijun Cao [2,3,5], Jianyong He [1,2,3,4,5,*] and Guosheng Li [2,3,5,*]

1 Zhengzhou Institute of Multipurpose Utilization of Mineral Resources, Chinese Academy of Geological Sciences, Zhengzhou 450006, China; wff18339196581@163.com (F.W.); liulei_9910@163.com (L.L.)
2 Zhongyuan Critical Metals Laboratory, Zhengzhou University, Zhengzhou 450001, China; zhangjingjing123@gs.zzu.edu.cn (J.Z.); yijuncao@zzu.edu.cn (Y.C.)
3 School of Chemical Engineering, Zhengzhou University, Zhengzhou 450001, China
4 Key Laboratory of Evaluation and Multipurpose Utilization of Polymetallic Ores, Ministry of Natural Resources, Zhengzhou 450006, China
5 The Key Laboratory of Critical Metals Minerals Supernormal Enrichment and Extraction, Ministry of Education, Zhengzhou 450001, China
* Correspondence: jianyong_he@zzu.edu.cn (J.H.); lgscumt@163.com (G.L.)
† These authors have equally contributed to this work.

Abstract: Lepidolite, crucial for lithium extraction, is primarily processed through flotation. However, conventional flotation inhibitors pose environmental challenges. This study introduces Fe(III) as a selective and eco-friendly inhibitor in lepidolite flotation. We investigated its impact on flotation performance and interaction mechanisms with feldspar, quartz, and lepidolite. Adsorption studies revealed that dodecylamine (DDA) selectively adsorbs onto lepidolite when Fe(III) is present. Consistent contact angle and flotation results showed reduced hydrophobicity and recovery rates for feldspar and quartz, with minimal impact on lepidolite. Zeta potential measurements indicated lower potentials for feldspar and quartz compared to lepidolite. Notably, the addition of Fe(III) altered the isoelectric points of quartz and feldspar, suggesting stronger Fe(III) adsorption on these minerals. Infrared spectroscopy and X-ray photoelectron spectroscopy confirmed reduced DDA adsorption on feldspar and quartz surfaces due to Fe(III) adsorption, while DDA adsorption on lepidolite remained largely unaffected. The mechanism underlying Fe(III)'s selective inhibition on feldspar and quartz involves their more negative surfaces compared to lepidolite, which facilitates Fe(III) adsorption and inhibits DDA adsorption. This study offers insights into mechanisms relevant to systems using metal ions as depressants, providing valuable references for similar research.

Keywords: lepidolite; flotation; depressant; ferric ion; zeta potential; feldspar; quartz

Citation: Wang, F.; Liu, L.; Zhang, J.; Cao, Y.; He, J.; Li, G. Selective Inhibition Mechanisms of Fe(III) in the Flotation of Lepidolite. *Minerals* **2024**, *14*, 851. https://doi.org/10.3390/min14090851

Academic Editor: Hyunjung Kim

Received: 22 July 2024
Revised: 10 August 2024
Accepted: 20 August 2024
Published: 23 August 2024

1. Introduction

Lithium, known for its lightweight and high mobility, plays a crucial role in energy storage devices, particularly in modern electric vehicles. The demand for lithium is projected to increase eightfold by 2040 [1]. To meet this escalating demand, efforts are underway to recover and recycle all potential lithium resources, including brines, lithium minerals, and retired lithium-ion batteries [2–5]. Given the limited production capacity of lithium extraction from brines, extracting lithium from hard rocks such as spodumene and lepidolite remains the primary method in many regions, including China and Australia [6,7]. Lepidolite, in particular, is a significant mineral source for lithium extraction, essential for easing the strain on lithium resource availability [8]. However, the raw lepidolite is extensively associated with quartz and feldspar resulting in low-grade minerals, which promote the challenge to effectively utilize refractory lepidolite resources [2].

Flotation is a powerful technology to separate fine minerals by enhancing the hydrophobicity difference between the purpose mineral and the gangue mineral surfaces in

a complex mineral pulp [9]. Lepidolite is primarily extracted via flotation from gangue minerals like feldspar and quartz [10,11]. The flotation collector is the most important reagent in mineral flotation. The flotation collector plays a pivotal role, with fatty amine collectors being common for lepidolite flotation, primarily adsorbing through electrostatic and hydrogen bonding interactions [12,13]. For instance, dodecylamine (DDA) is widely favored for its superior collecting ability in lepidolite flotation [14,15]. Individuals have applied DDA and its mixture with sodium oleate as selective collectors [16–18]. Moreover, to enhance flotation selectivity, inhibitors such as sodium silicate, sodium hexametaphosphate, and oxalic acid are used to depress feldspar and quartz [19–21]. However, these inhibitors often require large dosages, leading to lower flotation efficiency and increased costs. Issues like excessive sodium silicate in wastewater can cause significant settling problems, posing risks to water resources, ecological environments, and human health [22]. Therefore, there is a critical need to explore more environmentally friendly and efficient inhibitors.

Metal ions are widely utilized to modify mineral surface properties, aiming for high selectivity in flotation processes. Typically, metal ions act as activators by bridging collectors and mineral surfaces. For instance, Pb^{2+} [23–25] and Ca^{2+} [26] facilitate the attachment of hydroxamic or fatty acids to oxide minerals, enhancing surface hydrophobicity and improving flotation performance. Additionally, Ca^{2+}, Mg^{2+}, and Fe^{3+} have been reported as inhibitors in fine cassiterite flotation when octanohydroxamic acid is used as a collector. In these cases, $CaOH^{+}$, $MgOH^{+}$, and $Fe(OH)_3$ act as depressants due to their selective adsorption as metal hydroxide species [27]. Metal ions demonstrate diverse effects in oxide mineral flotation. For example, Fe^{3+} is commonly employed in spodumene flotation [28] but can also activate gangue minerals [29,30]. However, the underlying mechanisms behind these effects are not yet well revealed.

This study explores the use of Fe^{3+} as a depressant for achieving selective flotation separation of lepidolite from its gangue minerals (feldspar and quartz), employing DDA as a collector. Various experiments including adsorption studies, contact angle measurements, solution species analysis, Zeta potential measurements, infrared spectroscopy, and X-ray photoelectron spectroscopy (XPS) were conducted. These investigations aimed to elucidate the adsorption behaviors of Fe^{3+} and the selective inhibitory mechanisms of Fe^{3+} on feldspar and quartz. The findings of this research provide valuable insights into understanding similar systems where metal ions serve as depressants.

2. Materials and Methods

2.1. Materials

The pure mineral samples used were purchased from Yunnan Province, China, including lepidolite, feldspar, and quartz. The X-ray diffraction results in Figure 1 indicated that the purities of the three minerals were 95.79%, 99.18%, and 99.51%, respectively. Chemical assay of the used lepidolite, feldspar, and quartz have been tabulated in Tables 1–3. The Li_2O content of lepidolite reached 7.2%, which was close to the values reported in the literature [5,31]. After crushing, the samples were sieved into particles of +38−75 μm for flotation experiments. The samples were further ground to −5 μm using a triple-head grinding machine for subsequent characterization tests. Dodecylamine (DDA) was used as the collector, and hexahydrated ferric chloride was used as the flotation inhibitor, both purchased from Shanghai Yien Chemical Technology Co., Ltd. (Shanghai, China). HCl and NaOH were selected as pH regulators for the flotation experiments. All reagents used were of analytical grade. Pure water (with a resistivity of 18.25 MΩ·cm) was used in the experiments.

Table 1. Chemical assay of lepidolite (%).

Composition	Li_2O	SiO_2	Al_2O_3	K_2O	Rb_2O	MnO	Na_2O	Cs_2O	Fe_2O_3
Weight(%)	7.20	52.62	21.13	13.02	2.02	1.13	0.36	0.23	0.21

Table 2. Chemical assay of feldspar (%).

Composition	SiO_2	Al_2O_3	Na_2O	CaO	K_2O
Weight(%)	68.69	18.16	12.33	0.42	0.11

Table 3. Chemical assay of quartz (%).

Composition	SiO_2	Al_2O_3	P_2O_5	ZnO	CaO
Weight(%)	99.57	0.19	0.04	0.04	0.03

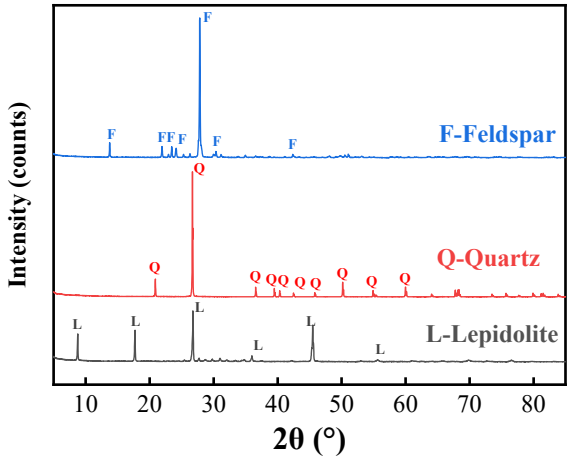

Figure 1. The X-ray diffraction spectrum of lepidolite, feldspar, and quartz.

2.2. Micro-Flotation

Pure mineral experiments were conducted in a 40 mL XFG single slot flotation machine (Wuhan Exploration Machinery Co., Ltd., Wuha, China), with a fixed flotation machine speed of 1700 r/min. Analytical balance was used for weighing, with 2 g of pure mineral weighed each time. The pure mineral was added to the flotation cell with an appropriate amount of deionized water and stirred for 2 min to fully suspend the mineral. pH adjuster (HCl or NaOH) was added using a micro syringe and stirred for 3 min, followed by the addition of the metal ion inhibitor and further stirring for 3 min. The collector was then added and stirred for 3 min, followed by a 4 min inflation and scraping time. The flotation product and the product in the tank were filtered and separated as concentrates and tailings, respectively. Then, the obtained samples were further placed in a blast drying oven for drying and weighing. Finally, the recovery rate of the mineral was calculated based on the mass of the pure mineral.

2.3. Contact Angle

The contact angle of the lepidolite surface was measured using a contact angle measuring instrument (Theta Flex, Sweden BioLins AB) (Biolin Scientific AB, Uusimaa, Finland). The surface of the pure mineral was polished flat and smoothed with sandpaper. The mineral samples were immersed in a solution containing hexahydrated ferric chloride and dodecylamine for 10 min, then placed in a 40 °C vacuum drying oven for drying. Subsequently, the contact angle was measured three times for each sample, and the average value was adopted for further analysis.

2.4. Zeta Potential

The Zeta potential of lepidolite was measured using an electrophoretic light scattering instrument (Zetasizer NanoZS90, Malvern Instruments Ltd., Worcestershire, UK). Samples of −5 μm pure mineral were used in Zeta potential analysis. For each test, 50 mg of pure mineral was placed in a 100 mL beaker and mixed with 50 mL of potassium nitrate (KCl or

KNO_3) solution (1×10^{-2} mol/L) to maintain the ionic strength of the solution. The pH of the mineral slurry was adjusted using dilute hydrochloric acid and sodium hydroxide solutions [32], followed by magnetic stirring for 15 min at different pH values. After 5 min of sedimentation, the supernatant was used for Zeta potential measurements. Zeta potential measurements were repeated three times, and the average value was taken as the final result.

2.5. Fe(III) Adsorption Amount

Based on the solution speciation analysis of flotation reagents, the adsorption of ferric ions on the mineral surface was predicated. First, flotation reagents were prepared as solutions. A total of 100 mg of pure mineral was added into a 100 mL volumetric flask, and 40 mL of deionized water was further added into the flask. Then, similar to the flotation process, the ferric ion and collector solutions were further added, and 5 min of stirring and 5 min of standing still were subsequently applied in this system. Finally, The supernatant in the upper layer of the flask was extracted by a syringe with a microporous filter membrane and used as the test sample.

2.6. Fourier-Transform Infrared Spectroscopy

The Fourier-transform infrared (FTIR) spectrometer (Nicolet iS20, Thermo Fisher Scientific, Waltham, MA, USA) was used for infrared spectroscopy testing of lepidolite. A total of 2 g of pure mineral (−5 μm) was placed in a flotation cell, and distilled water and flotation reagents were added sequentially to reach a volume of 40 mL. After thorough stirring, the mixture was filtered, and the mineral was repeatedly washed with deionized water during filtration. Subsequently, the sample was vacuum-dried at 40 °C, and then the prepared sample was thoroughly tested using the method of highly pure potassium bromide tableting.

2.7. X-ray Photoelectron Spectroscopy

X-ray photoelectron spectroscopy (XPS) measurements were conducted on lepidolite using a K-Alpha+ X-ray photoelectron spectrometer (Thermo Fisher Scientific, Waltham, MA, USA). A total of 2 g of pure mineral with a particle size of 38–75 μm was placed into a 40 mL flotation cell, and 35 mL of deionized water was added and stirred. The pH was adjusted to 4 using HCl and NaOH, and then reagents were added and stirred for 30 min. The sample was washed with deionized water filtered and finally dried in a 40 °C vacuum drying oven.

3. Results and Discussion

3.1. Adsorption Amounts of Fe(III)

Figure 2a shows the adsorption amount of Fe^{3+} on the three minerals in the presence of 20 mg/L DDA. The obtained results show that the adsorption of Fe^{3+} on lepidolite is 0.26 mg/g, which is much lower than the adsorption amounts of 1.21 and 1.22 mg/g for feldspar and quartz, respectively. This result indicates that Fe^{3+} has strong adsorption selectivity to interact with feldspar and quartz.

Figure 2b shows the recovery rates of lepidolite, feldspar, and quartz as a function of different pH with a dodecylamine concentration of 20 mg/L. As shown in Figure 2b, with the increase in pH, the flotation recovery rates of the three minerals show a consistent declining trend. Within the pH range of 4 to 10, lepidolite, feldspar, and quartz exhibit good floatability, with recovery rates exceeding 90%. Under acidic conditions, the recovery rate of lepidolite is higher than that of feldspar and quartz. However, the recovery of these minerals is still similar. These results suggest that the separation of the lepidolite from the gangue minerals under no depressants is fairly difficult.

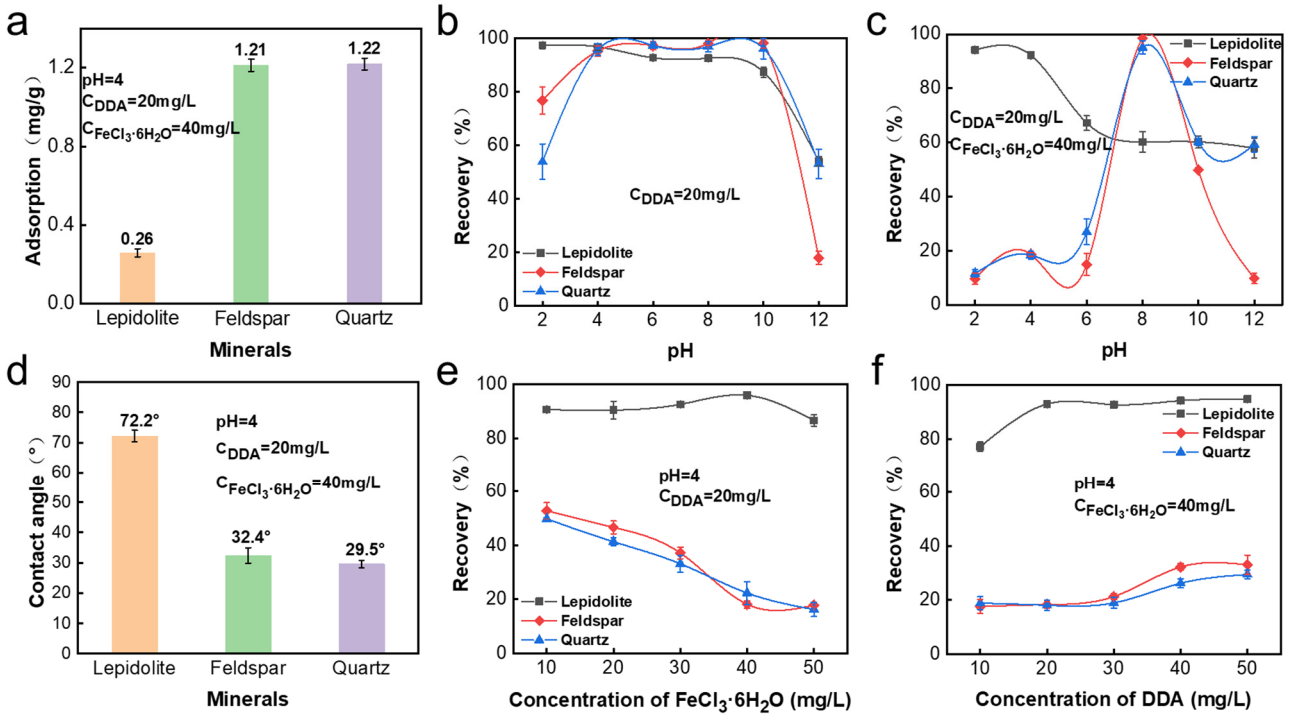

Figure 2. (**a**) Adsorption amount of Fe^{3+} on lepidolite, feldspar, and quartz. Flotation recovery rates of the three minerals using DDA as a function of pH in the (**b**) absence and (**c**) presence of $FeCl_3·6H_2O$. (**d**) Contact angles under the influence of $FeCl_3·6H_2O$ and DDA. (**e**) Flotation recovery of the three minerals at a DDA concentration of 20 mg/L as a function of $FeCl_3·6H_2O$ concentration. (**f**) Flotation recovery of the three minerals at 40 mg/L $FeCl_3·6H_2O$ as a function of DDA concentration.

Figure 2c shows the flotation recovery rates of lepidolite, feldspar, and quartz as a function of pH in the presence of Fe^{3+}. It can be seen that the recovery rate of lepidolite remains higher than 90% at a pH below 4, while the recovery rates of feldspar and quartz stay below 20%. The flotation recovery of lepidolite goes to lower values with the increase of pH higher than 4, while the flotation recovery of feldspar and quartz increases with the flotation pH and reaches their maximum points at pH = 8. These results show that within the pH range of 2 to 6, the recovery rate of lepidolite is significantly higher than that of feldspar and quartz. At pH = 8, the recovery rates of feldspar and quartz exceed that of lepidolite. As pH increases further, the recovery rates of feldspar and quartz drop sharply. Overall, at pH = 4, the flotation separation of lepidolite is most effective, with its recovery rate being 70% higher than that of feldspar and quartz, reaching 94.62%. This indicates that under acidic conditions, Fe^{3+} can significantly inhibit the flotation of feldspar and quartz.

Figure 2d shows the contact angles of lepidolite, feldspar, and quartz under optimal flotation conditions obtained from Figure 2b,c. The experimental results indicate that the contact angle of untreated lepidolite is only 24.1°, indicating its poor natural floatability. When treated with the cationic collector DDA and $FeCl_3·6H_2O$, the contact angle increased to 72.2° [17,33]. The contact angles of feldspar and quartz after reagent treatment were 32.4° and 29.5°, respectively. This suggests that feldspar and quartz exhibit stronger hydrophilicity after reagent treatment.

Figure 2e shows the flotation recovery rates of lepidolite, feldspar, and quartz as a function of the concentration of $FeCl_3·6H_2O$. The recovery rate of lepidolite remains stable at above 90%, while the recovery rates of feldspar and quartz gradually decrease. As the concentration of ferric chloride hexahydrate increases from 10 mg/L to 50 mg/L, the recovery rates of feldspar and quartz decrease from around 50% to below 20%. When the concentration of ferric chloride hexahydrate is 40 mg/L, the recovery rates of feldspar and quartz tend to stabilize, with the recovery rate of lepidolite being 95.31%.

Figure 2f shows the flotation recovery rates of lepidolite, feldspar, and quartz as a function of DDA concentrations. When the DDA concentration is 20 mg/L, the recovery rate of lepidolite reaches 92.85%, and as the DDA concentration increases, the recovery rate of lepidolite stabilizes. The recovery rates of feldspar and quartz show an increasing trend, reaching around 30% when the DDA concentration is 50 mg/L. It can be seen that the flotation result is optimal when the DDA concentration is 20 mg/L. At this point, the recovery rates of feldspar and quartz are 19.15% and 19.40%, respectively. The flotation and contact angle results indicate that Fe^{3+} can significantly inhibit the flotation of feldspar and quartz.

Adsorption and contact angle experiments reveal significantly higher Fe^{3+} adsorption on feldspar and quartz surfaces compared to lepidolite. Moreover, Fe^{3+} enhances the hydrophilicity of feldspar and quartz, indicating selective adsorption onto these minerals.

3.2. Solution Speciation and Zeta Potential Results

Figure 3a,b are the logarithmic concentration graphs of DDA (2×10^{-4} mol/L) and 1×10^{-4} mol/L Fe^{3+} as a function of pH values. The parameters used to draw the speciation diagrams are from references [34–36]. As shown in Figure 3a, when the solution pH is less than 9.69, DDA mainly exists in the forms of RNH_3^+ and $(RNH_3)^{2+}$ [34,35]. Since lepidolite typically has a negatively charged surface under the flotation pH, it provides a favorable condition for the adsorption of positively charged alkylamines. This also partially explains why dodecylamine can effectively float lepidolite under most pH conditions. When the solution pH is greater than 9.69, dodecylamine predominantly exists in the molecular forms of RNH_2(s) and RNH_2(aq), resulting in poorer flotation performance for lepidolite. Figure 3b shows the logarithmic concentration graph of Fe^{3+} (1×10^{-4} mol/L). Within an acidic pH range of 2 to 6, Fe^{3+}, $Fe(OH)^{2+}$, and $Fe(OH)_2^+$ are the main positive Fe species. Under these pH conditions, Fe^{3+} and positively charged hydroxy complexes exhibit electrostatic attractions to the negatively charged feldspar and quartz, thereby inhibiting the adsorption of collectors on their surfaces. According to the results of Fuerstenau et al. [37], when the pH is greater than 6, the solution mainly contains $Fe(OH)_3$ and $Fe(OH)_4^-$. At this pH, the adsorption effect of metal ions and their complexes on the mineral surfaces weakens, and the selective inhibition of feldspar and quartz essentially disappears. This result also indicates that the dimmish of the positive hydroxylated species should be responsible for the decrease of the flotation selectivity.

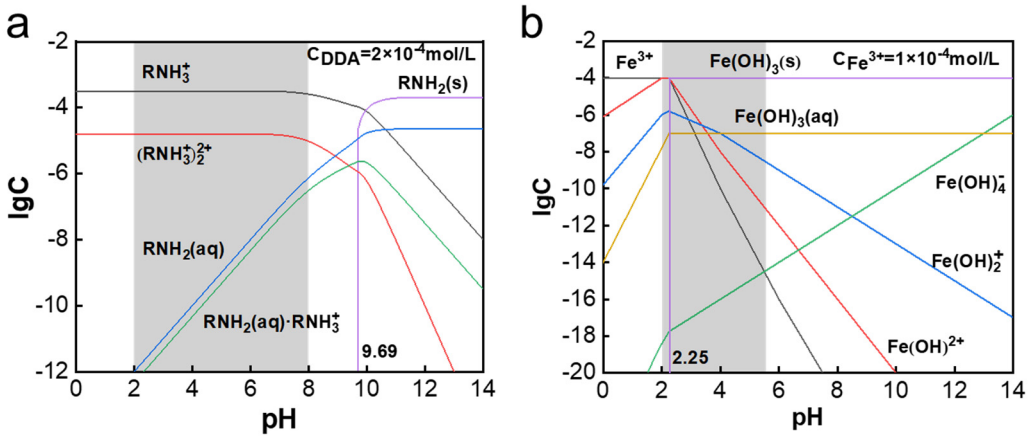

Figure 3. Solution speciation diagrams of (**a**) 2×10^{-4} mol/L DDA and (**b**) 1×10^{-4} mol/L Fe^{3+} as a function of pH.

Figure 4a shows the Zeta potential diagram of lepidolite before and after interaction with DDA and Fe^{3+}. As shown in Figure 4a, the isoelectric point (IEP) of lepidolite in water is approximately 2.5, and it carries a negative charge when the pH is higher than this point. This result is consistent with previous results [17,38]. When DDA and Fe^{3+} are added individually, the Zeta potential of lepidolite shifts in a positive direction. If DDA

and Fe^{3+} are added simultaneously, the positive shift of lepidolite is further enhanced. This indicates that both DDA and Fe^{3+} can adsorb on the surface of lepidolite, and the addition of Fe^{3+} does not significantly affect the adsorption of DDA. Figure 4b depicts the Zeta potential diagram of feldspar before and after the addition of DDA and Fe^{3+}. It can be seen that the isoelectric point of feldspar in aqueous solution is approximately 1.5. After the addition of DDA and Fe^{3+}, the Zeta potential of feldspar shifts in a positive direction. When Fe^{3+} is present, the Zeta potential of feldspar decreases rapidly at pH 6~12. This phenomenon is caused by the fact that Fe^{3+} mainly exists in the form of $Fe(OH)_3$ and $Fe(OH)^{4-}$ in the solution at pH > 6, thereby reducing the potential of the feldspar surface. When DDA and Fe^{3+} are added simultaneously, at pH 2 and 4, the Zeta potential of feldspar is consistent with that of Fe^{3+} presence, indicating that Fe^{3+} dominates the adsorption on feldspar. Figure 4c shows the surface zeta potential of quartz before and after the treatment of different reagents. It can be seen that in pure water, the zeta potential of quartz decreases with increasing slurry pH, with its isoelectric point at around pH = 1.2. When the cationic collector DDA is added, the zeta potential of quartz shifts in a positive direction, with its isoelectric point moving to around pH = 4. It can be inferred that the positively charged amine ions in the solution are adsorbed on the quartz surface. With the further increase of pH, the positive shift decreases due to the lower concentration of positively charged DDA in the solution, leading to weakened adsorption. In the presence of Fe^{3+}, the zeta potential of quartz shifts in a positive direction, and the shift is more pronounced under acidic conditions. At this time, Fe^{3+} exists in the solution in the forms of Fe^{3+} and $Fe(OH)^{2+}$, which increases the quartz surface potential by adsorbing onto the quartz surface. When both DDA and Fe^{3+} are present simultaneously, the shift of the quartz surface zeta potential is similar to that of feldspar. Under acidic conditions, Fe^{3+} can also inhibit the adsorption of DDA on the quartz surface.

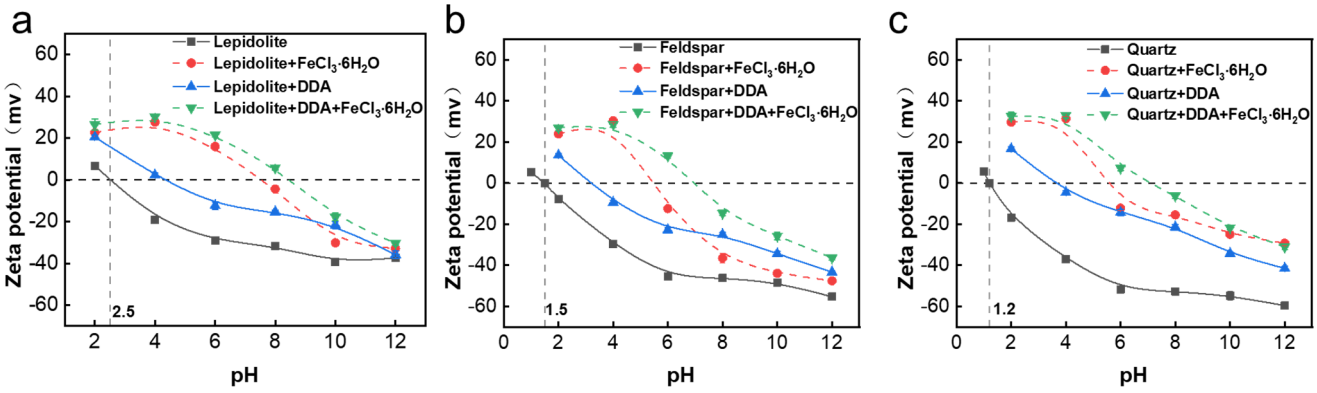

Figure 4. Zeta potential diagrams of (**a**) lepidolite, (**b**) feldspar, and (**c**) quartz minerals before and after the treatment of DDA, Fe^{3+}, and DDA + Fe^{3+}.

It can be seen from the above analysis that Fe^{3+} can actively adsorb onto the three minerals. The IEPs of the three minerals, from highest to lowest, are in the order of lepidolite > feldspar > quartz. Fe^{3+} can increase the IEPs of lepidolite from 2.5 to 4, feldspar from 1.5 to 3.2, and quartz from 1.2 to 3.8. Fe^{3+} adsorption has shown a higher influence on the adsorption of DDA on quartz and feldspar, where zeta potentials change more significantly compared to lepidolite.

3.3. FTIR Results

Figure 5a shows the infrared spectra results of lepidolite treated by DDA and DDA + Fe^{3+}, respectively. The characteristic peak at 761 cm^{-1} can be attributed to Al-O octahedral vibrations, and the peak at 468 cm^{-1} can be attributed to Si-O tetrahedral vibrations. These peaks at 761 cm^{-1} and 468 cm^{-1} can be assigned to lepidolite. After the addition of DDA, the peaks at 3331 cm^{-1} and 2956 cm^{-1} should be assigned to N-H stretching vibration peaks. Simultaneously, $-CH_3$ and $-CH_2$ stretching vibration absorption peaks can be seen at

2921 cm^{-1} and 2852 cm^{-1} [39,40], respectively, with strong peak intensities, indicating that DDA has adsorbed onto the surface of lepidolite. When $FeCl_3 \cdot 6H_2O$ was further introduced, the characteristic peaks of DDA remained strong, indicating that the presence of Fe^{3+} does not significantly affect the adsorption of DDA on lepidolite. This result corresponds well with the previous flotation test results.

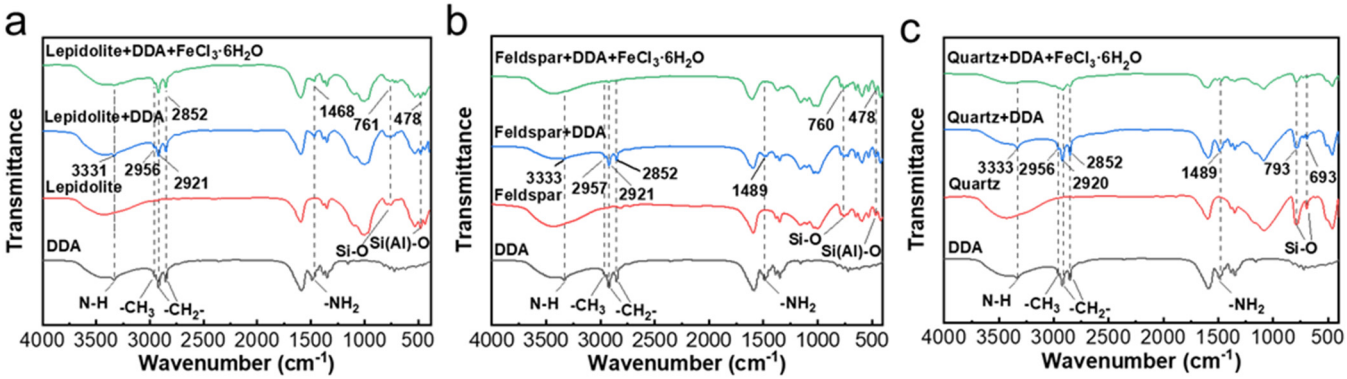

Figure 5. FTIR spectra of (**a**) lepidolite, (**b**) feldspar, and (**c**) quartz before and after the treatment of DDA and DDA + Fe^{3+}.

Figure 5b shows the infrared spectra results of feldspar treated by DDA and DDA + Fe^{3+}, respectively. As shown in Figure 5b, the characteristic peaks of feldspar are located at 1157 cm^{-1} and 1093 cm^{-1}, which can be assigned to the Si-O stretching vibration peaks. The peaks at 1039 cm^{-1} and 999 cm^{-1} can be attributed to the Si(Al)-O stretching vibration peaks. The peak at 760 cm^{-1} can be seen as the Si-O-Si symmetric stretching vibration peak. The peak at 648 cm^{-1} can be attributed to the O-Si-O stretching vibration peak. After the addition of DDA, N-H stretching vibration peaks can be observed at 3331 cm^{-1} and 2956 cm^{-1}. Simultaneously, $-CH_3$ and $-CH_2$ stretching vibration absorption peaks can be observed at 2921 cm^{-1} and 2852 cm^{-1}, respectively, with high peak intensities, indicating that DDA has a substantial adsorption on feldspar. When BHA was further added, no new characteristic peaks appeared. With the addition of $FeCl_3 \cdot 6H_2O$, the characteristic peaks of DDA weakened or even disappeared, indicating that the addition of metal iron ions inhibited the adsorption of the collector on feldspar. Combining the solution species of the reagents in Figure 3, it is speculated that the positively charged iron ions preferentially adsorb onto feldspar, inhibiting the adsorption of DDA on feldspar. The obtained results correspond well with the previous flotation test results.

Figure 5c shows the infrared spectra results of quartz treated by DDA and DDA + Fe^{3+}, respectively. As shown in Figure 5c, the characteristic peaks of quartz at 3429 cm^{-1} is the Si-OH hydroxyl stretching vibration peak; at 1881 cm^{-1} is the Si-O tetrahedral stretching vibration peak; at 1174 cm^{-1} and 1182 cm^{-1} are the Si-O bending vibration peaks; and at 793 cm^{-1}, 693 cm^{-1}, and 460 cm^{-1} are the bending vibration absorption peaks of O-Si-O and Si-O bonds. After the addition of DDA, N-H stretching vibration peaks appeared at 3333 cm^{-1} and 2956 cm^{-1}. Additionally, $-CH_3$ and $-CH_2$ stretching vibration absorption peaks appeared at 2920 cm^{-1} and 2852 cm^{-1}, respectively, with significant peak intensities, indicating that DDA has a strong adsorption effect on quartz. When BHA was further added, no new absorption peaks were produced. With the addition of $FeCl_3 \cdot 6H_2O$, the intensity of the characteristic peaks of the collector DDA weakened or even disappeared, indicating that the introduction of Fe^{3+} has inhibited the adsorption of DDA on quartz, which is consistent with the previous flotation test results.

3.4. XPS Results

Figure 6 shows the XPS spectra of the raw lepidolite before and after the treatment of Fe^{3+} and DDA + Fe^{3+}.

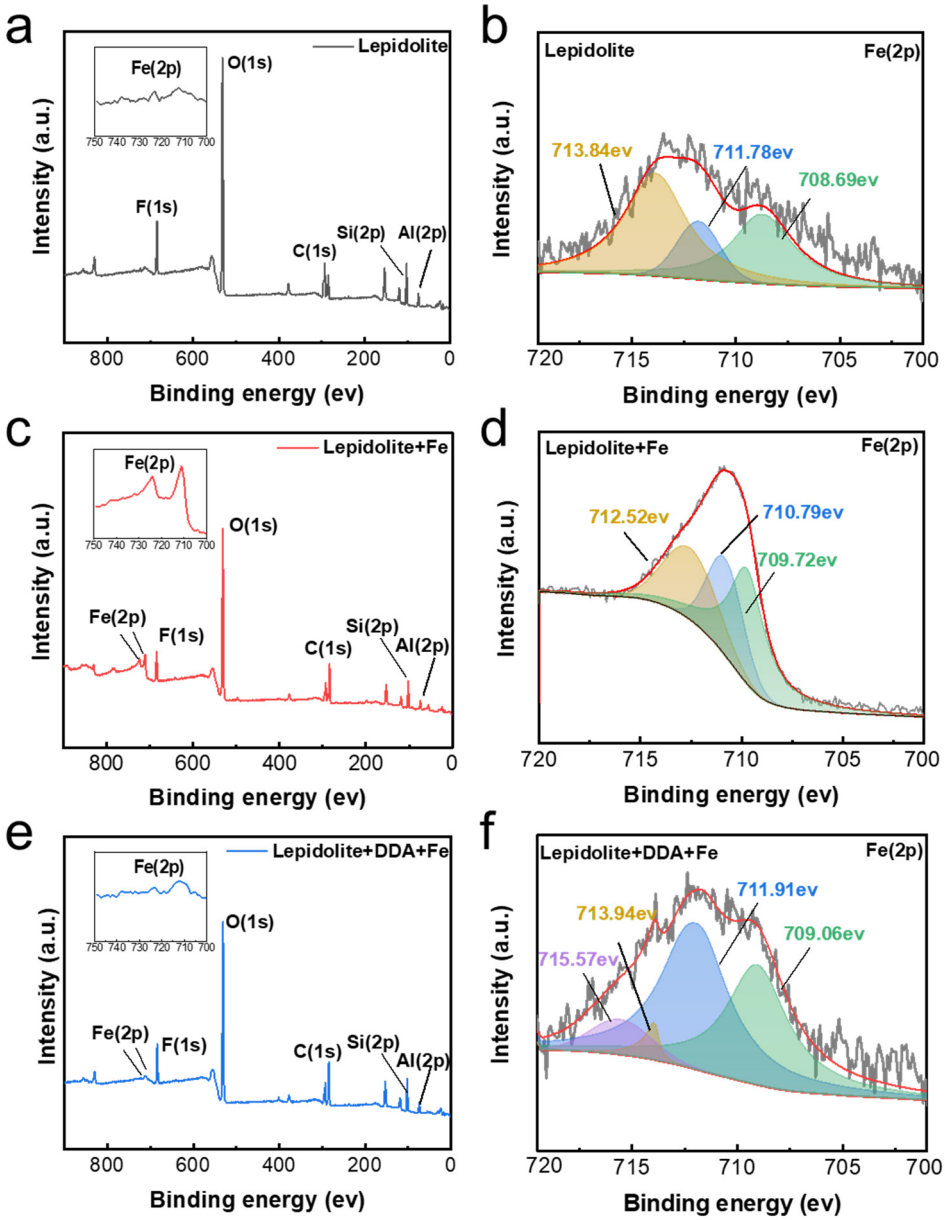

Figure 6. (**a**) The XPS survey spectrum of the pure lepidolite and (**b**) the high-resolution Fe(2p) spectrum. (**c**) The XPS survey spectrum of the Fe^{3+} treated lepidolite and (**d**) the high-resolution Fe(2p) spectrum. (**e**) The XPS survey spectrum of the DDA + Fe^{3+} treated lepidolite and (**f**) the high-resolution Fe(2p) spectrum.

As shown in Figure 6a, the characteristic peak of C(1s) has been detected in the raw lepidolite as a result of adventitious carbon [41], typically occurring within a few minutes of sample exposure to air. In the raw lepidolite sample in Figure 6a, characteristic peaks of Al2p, Si2p, O1s, F1s, etc., have been detected. After the addition of DDA and DDA + Fe^{3+}, the characteristic peak of N1s has been detected around 400 eV, as shown in Figure 6b,c, indicating the adsorption of the DDA on the surface of lepidolite. Additionally, no significant characteristic peaks of Fe2p have been detected in the raw lepidolite sample, whereas after the treatment of Fe^{3+}, significant characteristic peaks of Fe2p have been found at the binding energies of 710 to 740 eV [42,43], indicating that Fe^{3+} is adsorbed on the surface of lepidolite. After the treatment with DDA and $FeCl_3 \cdot 6H_2O$, lepidolite exhibits no characteristic peaks of Fe2p, suggesting that the adsorption is primarily dominated by DDA, thereby inhibiting the adsorption of Fe^{3+} elements onto lepidolite.

3.5. Selective Depressing Mechanism of Fe(III)

Figure 7 demonstrates Fe^{3+}'s pivotal role in selectively separating lepidolite from feldspar and quartz through selective adsorption. Adsorption experiments unequivocally reveal that Fe^{3+} markedly diminishes DDA adsorption on quartz and feldspar surfaces. Concurrent analyses via solution speciation, FTIR, and XPS consistently validate Fe^{3+}'s active adsorption on quartz and its interference with DDA adsorption. The selective adsorption of Fe^{3+} is chiefly driven by the minerals' strong negative surface charges, with lepidolite exhibiting the highest and quartz the lowest among the three minerals. Consequently, Fe^{3+} adsorption follows the sequence: quartz > feldspar > lepidolite. Increased Fe^{3+} adsorption on gangue minerals elevates their surface potentials and potentially alters surface oxygen, thereby significantly decreasing the adsorption of cationic collectors like DDA. These insights offer a comprehensive rationale for the flotation and contact angle results observed in this investigation.

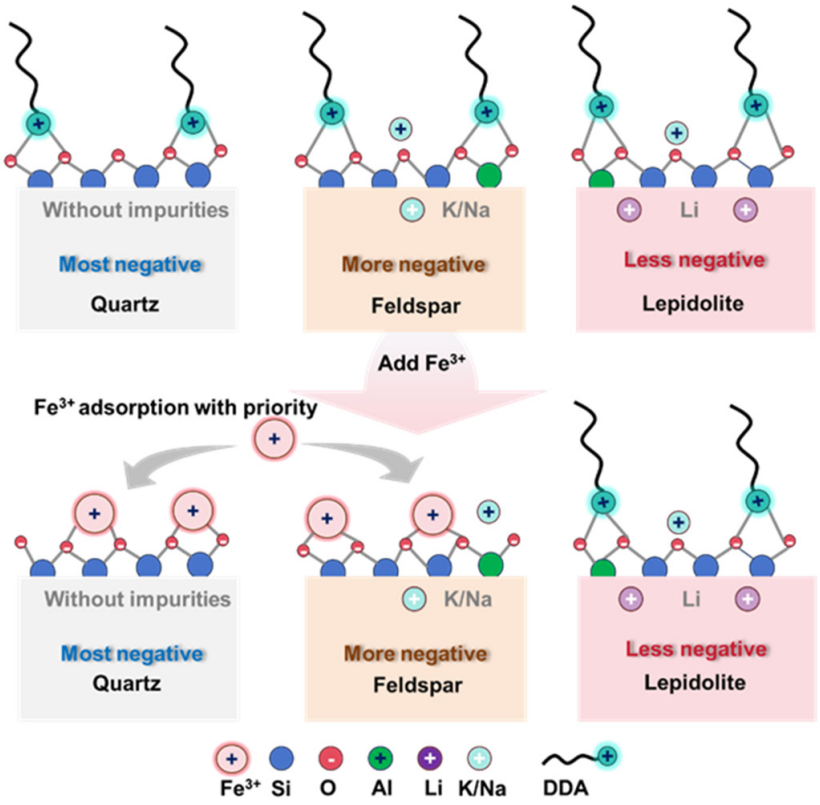

Figure 7. The proposed model for the utilization of Fe^{3+} as a selective depressant in the flotation of lepidolite from feldspar and quartz.

4. Conclusions

This manuscript proposes Fe^{3+} as an environmentally friendly inhibitor for feldspar and quartz in lepidolite mineral flotation. The study systematically investigates Fe^{3+}'s flotation performance and interaction mechanisms with these minerals through flotation tests, adsorption experiments, zeta potential measurements, FTIR analysis, and XPS tests. The flotation results demonstrate that Fe^{3+} reduces the recovery rates of feldspar and quartz to less than 20% while achieving a recovery rate of over 90% for lepidolite. Adsorption and contact angle experiments reveal significantly higher Fe^{3+} adsorption on feldspar and quartz surfaces compared to lepidolite. Moreover, Fe^{3+} enhances the hydrophilicity of feldspar and quartz, indicating selective adsorption onto these minerals. FTIR tests indicate that Fe^{3+} reduces DDA adsorption on feldspar and quartz surfaces, further confirming its inhibitory effect. XPS analysis shows predominant DDA adsorption on lepidolite in the presence of Fe^{3+}. The underlying mechanism of Fe^{3+}'s selective inhibition on feldspar and

quartz lies in their more negative surface potentials compared to lepidolite, facilitating Fe^{3+} adsorption and thereby inhibiting DDA adsorption. This finding provides valuable insights for similar systems using metal ions as effective and selective inhibitors in oxide mineral separation based on surface zeta potentials.

Author Contributions: Conceptualization, L.L., J.H., Y.C. and G.L.; methodology, J.H. and G.L.; validation, F.W., J.Z. and J.H.; formal analysis, F.W., J.Z. and J.H.; investigation, F.W., J.Z. and J.H.; resources, L.L., Y.C. and G.L.; data curation, F.W., J.Z. and J.H.; writing—original draft preparation, F.W., L.L. and J.H.; writing—review and editing, L.L., J.H. and G.L.; visualization, F.W. and J.Z.; supervision, J.H. and G.L.; project administration, J.H., Y.C. and G.L.; funding acquisition, J.H., Y.C. and G.L. All authors have read and agreed to the published version of the manuscript.

Funding: This research was funded by the National Natural Science Foundation of China (Grants 52374281 and 52204287), the Postdoctoral Fellowship Program of CPSF (Grant GZC20232398), the China Postdoctoral Science Foundation (Grant 2023TQ0302), the Research Startup Fund of Zhengzhou University (Grant 32213512), the Project of Zhongyuan Critical Metals Laboratory (Grants GJJSGFYQ202316 and GJJSGFYQ202322), and the Open Research Fund of the Key Laboratory of Multi-metal Ore Evaluation and Comprehensive Utilization of the Ministry of Land and Resources.

Data Availability Statement: Raw data for this work are available upon reasonable request from the corresponding authors.

Acknowledgments: The authors appreciate the support from the Key Laboratory of Evaluation and Multipurpose Utilization of Polymetallic Ores of the Ministry of Natural Resources, Zhengzhou, China.

Conflicts of Interest: The authors declare no conflicts of interest.

References

1. Maisel, F.; Neef, C.; Marscheider-Weidemann, F.; Nissen, N.F. A Forecast on Future Raw Material Demand and Recycling Potential of Lithium-Ion Batteries in Electric Vehicles. *Resour. Conserv. Recycl.* **2023**, *192*, 106920. [CrossRef]
2. Korbel, C.; Filippova, I.V.; Filippov, L.O. Froth Flotation of Lithium Micas—A Review. *Miner. Eng.* **2023**, *192*, 107986. [CrossRef]
3. Tabelin, C.B.; Dallas, J.; Casanova, S.; Pelech, T.; Bournival, G.; Saydam, S.; Canbulat, I. Towards a Low-Carbon Society: A Review of Lithium Resource Availability, Challenges and Innovations in Mining, Extraction and Recycling, and Future Perspectives. *Miner. Eng.* **2021**, *163*, 106743. [CrossRef]
4. Xie, R.; Zhao, Z.; Tong, X.; Xie, X.; Song, Q.; Fan, P. Review of the Research on the Development and Utilization of Clay-Type Lithium Resources. *Particuology* **2024**, *87*, 46–53. [CrossRef]
5. Li, H.; Eksteen, J.; Kuang, G. Recovery of Lithium from Mineral Resources: State-of-the-Art and Perspectives—A Review. *Hydrometallurgy* **2019**, *189*, 105129. [CrossRef]
6. Xie, R.; Zhu, Y.; Liu, J.; Li, Y.; Wang, X.; Shumin, Z. Research Status of Spodumene Flotation: A Review. *Miner. Process. Extr. Metall. Rev.* **2021**, *42*, 321–334. [CrossRef]
7. Tadesse, B.; Makuei, F.; Albijanic, B.; Dyer, L. The Beneficiation of Lithium Minerals from Hard Rock Ores: A Review. *Miner. Eng.* **2019**, *131*, 170–184. [CrossRef]
8. Zhang, S.; Huang, Z.; Wang, H.; Liu, R.; Cheng, C.; Shuai, S.; Hu, Y.; Guo, Z.; Yu, X.; He, G.; et al. Flotation Performance of a Novel Gemini Collector for Kaolinite at Low Temperature. *Int. J. Min. Sci. Technol.* **2021**, *31*, 1145–1152. [CrossRef]
9. Fuerstenau, D.W. Pradip A Century of Research Leading to Understanding the Scientific Basis of Selective Mineral Flotation and Design of Flotation Collectors. *Min. Metall. Explor.* **2019**, *36*, 3–20. [CrossRef]
10. Huang, Z.; Shuai, S.; Burov, V.E.; Poilov, V.Z.; Li, F.; Wang, H.; Liu, R.; Zhang, S.; Cheng, C.; Li, W.; et al. Adsorption of Trisiloxane Surfactant for Selective Flotation of Scheelite from Calcite at Room Temperature. *Langmuir* **2022**, *38*, 9010–9020. [CrossRef] [PubMed]
11. Shu, K.; Xu, L.; Wu, H.; Xu, Y.; Luo, L.; Yang, J.; Tang, Z.; Wang, Z. In Situ Adsorption of Mixed Anionic/Cationic Collectors in a Spodumene-Feldspar Flotation System: Implications for Collector Design. *Langmuir* **2020**, *36*, 8086–8099. [CrossRef] [PubMed]
12. Wang, H.; Wang, L.; Yang, S.; Liu, C.; Xu, Y. Investigations on the Reverse Flotation of Quartz from Hematite Using Carboxymethyl Chitosan as a Depressant. *Powder Technol.* **2021**, *393*, 109–115. [CrossRef]
13. Liu, X.; Xie, J.; Huang, G.; Li, C. Low-Temperature Performance of Cationic Collector Undecyl Propyl Ether Amine for Ilmenite Flotation. *Miner. Eng.* **2017**, *114*, 50–56. [CrossRef]
14. Yang, B.; Fu, Y.F.; Yin, W.Z.; Sheng, Q.Y.; Zhu, Z.L.; Yin, X.M. Selective Collection Performance of an Efficient Quartz Collector and Its Response to Flotation Separation of Malachite from Quartz. *Miner. Eng.* **2021**, *172*, 107174. [CrossRef]
15. Bulatovic, S.M. Handbook of Flotation Reagents: Chemistry, Theory and Practice Flotation of Industrial Minerals(II). In *Handbook of Flotation Reagents: Chemistry, Theory and Practice Flotation of Sulfide Ores*; Elsevier Science & Technology Books: Peterborough, UK, 2015; p. 459, ISBN 9780444530295.

16. Xu, L.; Wu, H.; Dong, F.; Wang, L.; Wang, Z.; Xiao, J. Flotation and Adsorption of Mixed Cationic/Anionic Collectors on Muscovite Mica. *Miner. Eng.* **2013**, *41*, 41–45. [CrossRef]
17. Wei, Q.; Feng, L.; Dong, L.; Jiao, F.; Qin, W. Selective Co-Adsorption Mechanism of a New Mixed Collector on the Flotation Separation of Lepidolite from Quartz. *Colloids Surf. A Physicochem. Eng. Asp.* **2021**, *612*, 125973. [CrossRef]
18. Huang, Z.; Zhang, S.; Cheng, C.; Wang, H.; Liu, R.; Hu, Y.; He, G.; Yu, X.; Fu, W. Recycling Lepidolite from Tantalum-Niobium Mine Tailings by a Combined Magnetic-Flotation Process Using a Novel Gemini Surfactant: From Tailings Dams to the "Bling" Raw Material of Lithium. *ACS Sustain. Chem. Eng.* **2020**, *8*, 18206–18214. [CrossRef]
19. Marion, C.; Li, R.; Waters, K.E. A Review of Reagents Applied to Rare-Earth Mineral Flotation. *Adv. Colloid. Interface Sci.* **2020**, *279*, 102142. [CrossRef]
20. Chen, Z.; Ren, Z.; Gao, H.; Zheng, R.; Jin, Y.; Niu, C. Flotation Studies of Fluorite and Barite with Sodium Petroleum Sulfonate and Sodium Hexametaphosphate. *J. Mater. Res. Technol.* **2019**, *8*, 1267–1273. [CrossRef]
21. Ramirez, A.; Rojas, A.; Gutierrez, L.; Laskowski, J.S. Sodium Hexametaphosphate and Sodium Silicate as Dispersants to Reduce the Negative Effect of Kaolinite on the Flotation of Chalcopyrite in Seawater. *Miner. Eng.* **2018**, *125*, 10–14. [CrossRef]
22. Kang, J.; Sun, W.; Hu, Y.; Gao, Z.; Liu, R.; Zhang, Q.; Liu, H.; Meng, X. The Utilization of Waste By-Products for Removing Silicate from Mineral Processing Wastewater via Chemical Precipitation. *Water Res.* **2017**, *125*, 318–324. [CrossRef] [PubMed]
23. He, J.; Sun, W.; Chen, D.; Gao, Z.; Zhang, C. Interface Interaction of Benzohydroxamic Acid with Lead Ions on Oxide Mineral Surfaces: A Coordination Mechanism Study. *Langmuir* **2021**, *37*, 3490–3499. [CrossRef] [PubMed]
24. He, J.; Sun, W.; Zeng, H.; Fan, R.; Hu, W.; Gao, Z. Unraveling Roles of Lead Ions in Selective Flotation of Scheelite and Fluorite from Atomic Force Microscopy and First-Principles Calculations. *Miner. Eng.* **2022**, *179*, 107424. [CrossRef]
25. Miao, Y.; He, J.; Zhu, X.; Zhu, G.; Cao, S.; Fan, G.; Li, G.; Cao, Y. Hardness of Surface Hydroxyls and Its Pivotal Role in the Flotation of Cassiterite from Quartz via Lead Ions Activation. *Sep. Purif. Technol.* **2024**, *347*, 127565. [CrossRef]
26. Hu, Y.; He, J.; Zhang, C.C.; Zhang, C.C.; Sun, W.; Zhao, D.; Chen, P.; Han, H.; Gao, Z.; Liu, R.; et al. Insights into the Activation Mechanism of Calcium Ions on the Sericite Surface: A Combined Experimental and Computational Study. *Appl. Surf. Sci.* **2018**, *427*, 162–168. [CrossRef]
27. Ren, L.; Qiu, H.; Qin, W.; Zhang, M.; Li, Y.; Wei, P. Inhibition Mechanism of Ca^{2+}, Mg^{2+} and Fe^{3+} in Fine Cassiterite Flotation Using Octanohydroxamic Acid. *R. Soc. Open Sci.* **2018**, *5*, 180158. [CrossRef]
28. Tian, M.; Liu, R.; Gao, Z.; Chen, P.; Han, H.; Wang, L.; Zhang, C.; Sun, W.; Hu, Y. Activation Mechanism of Fe (III) Ions in Cassiterite Flotation with Benzohydroxamic Acid Collector. *Miner. Eng.* **2018**, *119*, 31–37. [CrossRef]
29. Fuerstenau, M.C.; Miller, J.D.; Pray, R.E.; Perinne, B.F. Metal Ion Activation in Xanthate Flotation of Quartz. *Min. Eng.* **1966**, *235*, 359–365.
30. He, J.; Zhang, Y.; Wang, F.; Wu, Y.; Cao, Y.; Li, G.; Gao, Z. Interaction Mechanisms of Typical Collectors with Zircon Surfaces and Their Influence on Surface Morphology and Hydrophobicity for Selective Flotation. *Appl. Surf. Sci.* **2024**, *648*, 158941. [CrossRef]
31. Christmann, P.; Gloaguen, E.; Labbé, J.F.; Melleton, J.; Piantone, P. Global Lithium Resources and Sustainability Issues. In *Lithium Process Chemistry: Resources, Extraction, Batteries, and Recycling*; Elsevier: Amsterdam, The Netherlands, 2015.
32. Fuerstenau, D.W. Pradip Zeta Potentials in the Flotation of Oxide and Silicate Minerals. *Adv. Colloid. Interface Sci.* **2005**, *114–115*, 9–26. [CrossRef]
33. Berger, O.; Ortial, S.; Wein, S.; Denoyelle, S.; Bressolle, F.; Durand, T.; Escale, R.; Vial, H.J.; Vo-Hoang, Y. Evaluation of Amidoxime Derivatives as Prodrug Candidates of Potent Bis-Cationic Antimalarials. *Bioorg Med. Chem. Lett.* **2019**, *29*, 2203–2207. [CrossRef] [PubMed]
34. Liu, J.; Wen, S.; Feng, Q.; Zhang, Q.; Wang, Y.; Zhou, Y.; Nie, W. Mechanism of Depression by Fe3+ During Hemimorphite Flotation. *Minerals* **2020**, *10*, 790. [CrossRef]
35. Ruan, Y.; Zhang, Z.; Luo, H.; Xiao, C.; Zhou, F.; Chi, R. Effects of Metal Ions on the Flotation of Apatite, Dolomite and Quartz. *Minerals* **2018**, *8*, 141. [CrossRef]
36. Gao, Z.; Sun, W.; Hu, Y. New Insights into the Dodecylamine Adsorption on Scheelite and Calcite: An Adsorption Model. *Miner. Eng.* **2015**, *79*, 54–61. [CrossRef]
37. Fuerstenau, M.C.; Lopez-Valdivieso, A.; Fuerstenau, D.W. Role of Hydrolyzed Cations in the Natural Hydrophobicity of Talc. *Int. J. Miner. Process* **1988**, *23*, 161–170. [CrossRef]
38. Zhang, H.; Chai, W.; Cao, Y. Flotation Separation of Quartz from Gypsum Using Benzyl Quaternary Ammonium Salt as Collector. *Appl. Surf. Sci.* **2022**, *576*, 151834. [CrossRef]
39. Huang, Z.; Shuai, S.; Wang, H.; Liu, R.; Zhang, S.; Cheng, C.; Hu, Y.; Yu, X.; He, G.; Fu, W. Froth Flotation Separation of Lepidolite Ore Using a New Gemini Surfactant as the Flotation Collector. *Sep. Purif. Technol.* **2022**, *282*, 119122. [CrossRef]
40. Xie, R.; Zhu, Y.; Liu, J.; Li, Y. A Self-Assembly Mixed Collector System and the Mechanism for the Flotation Separation of Spodumene from Feldspar and Quartz. *Miner. Eng.* **2021**, *171*, 107082. [CrossRef]
41. Keszthelyi, T.; Pászti, Z.; Rigó, T.; Hakkel, O.; Telegdi, J.; Guczi, L. Investigation of Solid Surfaces Modified by Langmuir-Blodgett Monolayers Using Sum-Frequency Vibrational Spectroscopy and X-Ray Photoelectron Spectroscopy. *J. Phys. Chem. B* **2006**, *110*, 8701–8714. [CrossRef]

42. Feng, Q.; Zhao, W.; Wen, S.; Cao, Q. Activation Mechanism of Lead Ions in Cassiterite Flotation with Salicylhydroxamic Acid as Collector. *Sep. Purif. Technol.* **2017**, *178*, 193–199. [CrossRef]
43. Pongpaiboonkul, S.; Phokharatkul, D.; Hodak, J.H.; Wisitsoraat, A.; Hodak, S.K. Enhancement of H2S-Sensing Performances with Fe-Doping in $CaCu_3Ti_4O_{12}$ Thin Films Prepared by a Sol-Gel Method. *Sens. Actuators B Chem.* **2016**, *224*, 118–127. [CrossRef]